In Situ Small Angle Neutron Scattering Revealing Ion Sorption in Microporous Carbon Electrical Double Layer Capacitors

Sofiane Boukhalfa,[†] Daniel Gordon,[†] Lilin He,[‡] Yuri B. Melnichenko,[‡] Naoki Nitta,[†] Alexandre Magasinski,[†] and Gleb Yushin[†,*]

[†]Department of Materials Science and Engineering, Georgia Institute of Technology, Atlanta, Georgia 30332, United States and [‡] Biology and Soft Matter Division, Neutron Sciences Directorate, Oak Ridge National Laboratory, Oak Ridge, Tennessee 37830, United States

ABSTRACT Experimental studies showed the impact of the electrolyte solvents on both the ion transport and the specific capacitance of microporous carbons. However, the related structure—property relationships remain largely unclear and the reported results are inconsistent. The details of the interactions of the charged carbon pore walls with electrolyte ions and solvent molecules at a subnanometer scale are still largely unknown. Here for the first time we utilize *in situ* small angle neutron scattering (SANS) to reveal the electroadsorption of organic electrolyte ions in carbon pores of different sizes. A 1 M solution of tetraethylammonium tetrafluoroborate (TEATFB) salt in deuterated acetonitrile (d-AN) was used in an activated carbon with the pore size distribution similar to that of the carbons used in commercial double layer capacitors. In spite of the incomplete wetting of the smallest carbon pores by the d-AN, we observed enhanced ion sorption in subnanometer pores under the applied potential. Such results suggest the visible impact of electrowetting phenomena counterbalancing the high energy of the carbon/electrolyte interface in small pores. This behavior may explain the characteristic butterfly wing shape of the cyclic voltammetry curve that demonstrates higher specific capacitance at higher applied potentials, when the smallest pores become more accessible to electrolyte. Our study outlines a general methodology for studying various organic salts—solvent—carbon combinations.

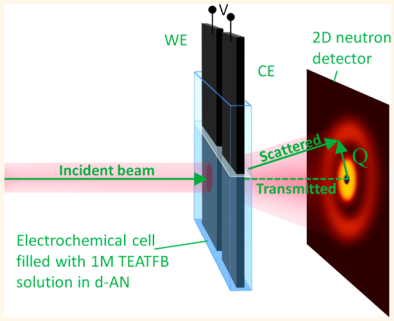

KEYWORDS: ion adsorption · small-angle neutron scattering · energy storage · porous carbon

Electroadsorption of organic electrolyte ions in microporous carbons under applied potential controls the performance and energy storage characteristics of commercial double layer capacitors (EDLCs) utilized in off-shore wind turbine systems, smart grid, uninterruptable power supplies, energy efficient industrial equipment, such as harbor cranes, lifts and forklifts, hybrid engines and electronic devices.[1−3]

One of the first studies of the pore size effect on electrolyte—carbon pore interactions revealed that a distortion of solvation shells is dependent on both the ion and the solvent.[4] The following studies of porous carbons having different average pore size suggested significant enhancement of the surface area normalized specific capacitance in small carbon micropores, where the ion solvation shells become highly distorted and the average charge separation distances between the ion centers and the pore walls decrease.[5,6] However, the dependence of the specific capacitance on the carbon microstructure[7] and functional groups,[8] the difference in the accessibility of pores by gas molecules (utilized for the surface area measurements) and by electrolyte ions, the lack of sufficiently accurate models capable to deduce the carbon specific surface area and pore size distribution from the gas sorption measurements assuming realistic shape of the pores,[9] and finally the variations in the electrode preparation procedure (where some of the pores could be blocked by the excess amount of a polymer binder or by collapsed pores in case when excessive pressure is applied) may distort the observed dependencies.[10,11]

Some insights about the ion adsorption in carbon pores could be extracted from NMR studies.[12−15] The first solid-state ^{11}B NMR

* Address correspondence to yushin@gatech.edu.

Received for review November 25, 2013 and accepted February 18, 2014.

Published online February 18, 2014
10.1021/nn406077n

© 2014 American Chemical Society

studies of BF_4^- anions of TEATFB confined in activated carbon pores showed significant upshift of the ^{11}B peak compared to that of free electrolyte, particularly in the smallest pores.[12] Similar observations were made by the follow up studies of Wang *et al.*[13] The authors distinguished two ^{11}B peaks and assigned them to ions present in small and large pores.[13] Interestingly, NMR studies on porous carbons with dual pore size distribution showed a single NMR peak.[14] The authors explained this observation by the rapid exchange of the BF_4^- anions between the closely located 1 and 4 nm pores of the utilized well-structured carbon.[14] Another interesting observation was that removal (drying) of electrolyte solvent diminished the average ion-wall distance in large pores, but did not affect such a distance in small pores,[14] providing an experimental evidence of the stripping of the solvation shells around the ions in the smallest pores.

Computer modeling and calculations offer complementary means to study ion adsorption phenomena.[16−26] However, the assumptions and parameters used in each of the described models may significantly affect the obtained results. In addition, the impacts of the realistic pore structure[22] and electrolyte solvent − carbon pore wall interactions on the predicted results may be significant.

Many of the factors that affect both the transport and the electroadsorption of ions in the carbon nanopores, such as electrolyte wetting, viscosity, dielectric constant, solvation energy of ions, size of the solvation shells and conductivity are also influenced by the electrolyte solvent. While these factors have been acknowledged to affect the performance of EDLCs,[1] neither has an in-depth understanding of their impacts been identified, nor any prognostic abilities been developed. In fact, comparison of acetonitrile (AN) *versus* a less polar (yet with higher dielectric constant) propylene carbonate (PC) solvent showed inconsistently either higher[27,28] or lower capacitance[29] in combination with the same salt, but depending on the porous carbon.

In our recent studies, we pioneered the use of small angle neutron scattering (SANS) to directly visualize proton adsorption in microporous carbons under variable potentials applied in aqueous (H_2O and D_2O) solutions.[30] In case of H_2O-based electrolyte that wetted well the carbon surface, we observed enhanced proton adsorption in subnanometer pores, while in case of D_2O-based electrolyte that did not wet some of the smallest pores, we observed greatly diminished proton adsorption in such pores.

In the current study, we aimed to further utilize the high penetrating power of neutrons and high cross section of neutron scattering on H in combination with the high neutron absorption cross section of B to reveal the pore size dependencies of electroadsorption of ions from H-containing and B-containing tetraethyl ammonium tetrafluoroborate (TEATFB) salt solution in AN. The observed ability to monitor the changes in the ion concentration in carbon pores of different size may open the door to a quantitative analysis and better understanding of the solvent effects, thus demystifying many of the described above phenomena related to electrolyte nanoconfinement under an applied electric field. We shall emphasize that in contrast to many prior studies, where the impact of pore size was studied by analyzing completely different carbons,[5,6,10,11] our experiments allow unambiguous observation of the different ion adsorption in various pores of the same material.

RESULTS AND DISCUSSION

Carbon Characterization. To avoid any impacts of the polymer binder on both the neutron scattering and the ion electrosorption, we have utilized a binder-free activated carbon fabric (ACF) for our study. Scanning electron microscopy (SEM) studies show long interwoven strands of individual carbon fibers of 10−15 μm in diameter (Figure 1a). High resolution transmission electron microscopy (TEM) analysis revealed a highly disordered carbon microstructure with small pore below 2 nm in size distinguishable at the very edges of the TEM samples (Figure 1b, top). No contamination could be detected.

X-ray diffraction (XRD) analysis confirmed the results of TEM studies and showed a pattern very typical for highly disordered carbons (Figure 2a). The two very broad yet visible peaks could be assigned to diffraction on (002) and (101) family of planes of disordered graphite. The N_2 adsorption/desorption isotherms collected at 77K were utilized to calculate the pore size distribution (Figure 2b) assuming the slit shape of the pores, which is a typical assumption for activated carbons.[31−33] Nearly all of the pores are within 0.4−2 nm in characteristic dimensions, similarly to that of the microporous activated carbon (AC) powder

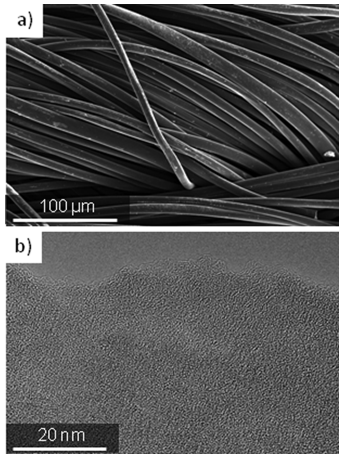

Figure 1. Electron microscopy of the ACF samples: (a) SEM micrograph showing morphology and diameter of the individual fibers; (b) high resolution TEM micrograph showing the disordered microstructure and micropores present within the activated carbon of ACF.

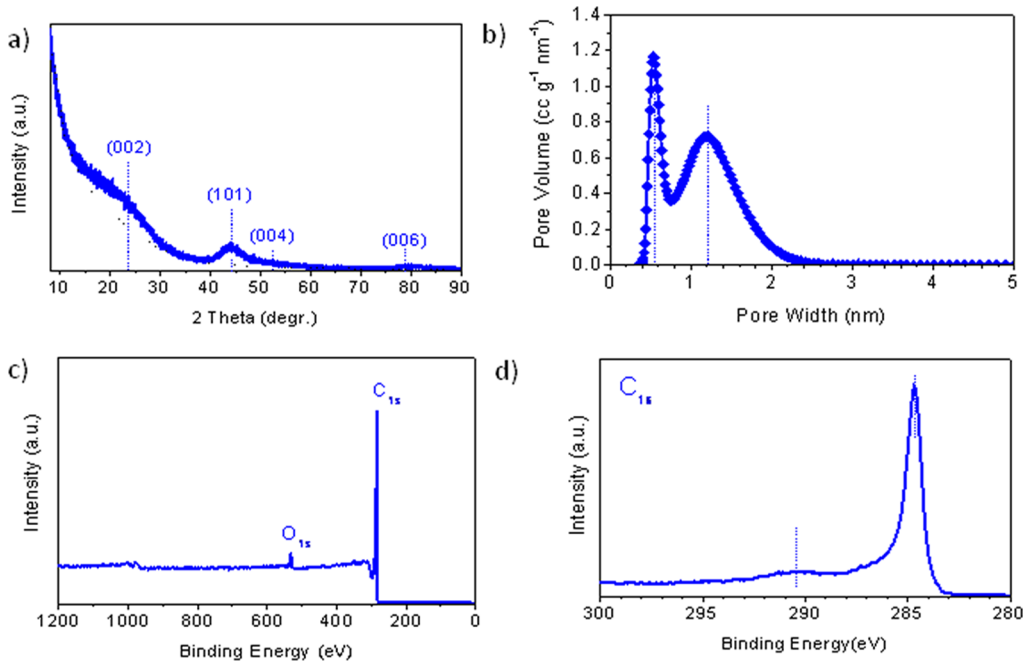

Figure 2. Characterization of the physical and chemical properties of the ACF samples: (a) XRD pattern, (b) pore size distribution, (c) survey, and (d) fine structure C_{1s} XPS spectra.

utilized in the majority of commercial EDLCs. X-ray photoelectron spectroscopy (XPS) was used to investigate the possible presence of functional groups on the surface of the electrodes. Such groups may induce Faradaic reduction−oxidation (redox) reactions[8,34] and thus affect the specific capacitance of the electrodes as well as the distribution of electrolyte and ions within the ACF pores. As expected, the XPS studies showed only a very minor content of oxygen present in the ACF samples (3 atom %, Figure 2c,d), similar to that of AC powders commonly used in commercial devices. Raman spectroscopy analysis (not shown for brevity) similarly demonstrated very similar microstructure of ACF and commercial AC powders. As such, we conclude that the selected ACF may serve as an excellent model system for our studies.

Electrochemical Measurements. A 1 M solution of TEATFB in AN is a common electrolyte of many commercial EDLCs. However, to improve the sensitivity of the SANS experiments to hydrogen, we had to select a deuterated version of the solvent (d-AN) for *in situ* SANS measurements. An ideal EDLC, having an infinitely small real component of complex impedance, shall exhibit the CV curves of a perfect rectangular shape[34] with a constant current or capacitance measured at all of the applied voltages. The CV studies of the actual porous carbon electrodes provide information about the relative ion storage capacities as well as the ion transport kinetics. The distortion of the CV curves at the transient regions, where the current directions are abruptly inversed (top left and bottom right portion of the curves, Figure 3) is mostly related to the ionic component of the EDLC resistance,

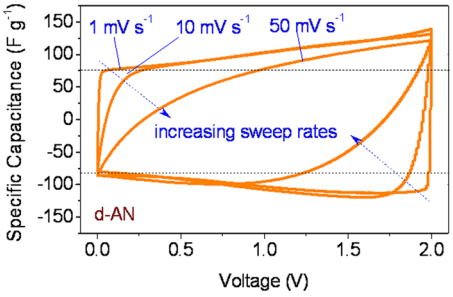

Figure 3. Electrochemical characterization of the ACF electrodes in a symmetric two-electrode setup using 1 M TEATFB/d-AN electrolyte: CV measurements collected at three different sweep rates, 1, 10, and 50 mV·s^{-1}, showing a significant distortion of the rectangular shape of an "ideal" EDLC for all measurements. A "butterfly wing" shape is clearly observed at slower sweep rates.

originating, in our case, from the limited rate of ion transport within the relatively large diameter of the ACF having a small average pore size (Figure 2b) and possibly some bottleneck pores present.

Increasing capacitance at higher values of the applied voltage (Figure 3) and forming so-called "butterfly wing" or "V" or "U" or "dumbbell" shape of the CV curves can be observed in various types of carbon electrodes, including organic or ionic liquid electrolytes which permit larger maximum voltage and in some cases in neutral aqueous electrolytes.[35−37] Various research groups offered different explanations to the observed deviations from the rectangular shape.

One of the earliest discussions on the experimentally observed dependence of capacitance on carbon electrode potential was initiated by Randin *et al.* while investigating the double layer formation on a basal

plane of pyrolytic graphite.[38] The capacitance of a graphite/electrolyte interface (we will call it a double layer capacitance, C_{DL}) was approximated by two components in a series: the capacitance of a space charge within graphite (C_{SC}) and the capacitance of an electrolyte layer (C_e). Assuming that the latter should be independent of the electrode itself (and thus could be approximated by relatively high values of $\sim$20 μF/cm^2 observed on the metal surfaces), Randin *et al.* suggested that the overall capacitance must be governed by the C_{SC}, as the smallest of the two, according to their estimations. If the expression for C_{SC} within a graphite electrode sample can be approximated by that for a pure intrinsic semiconductor, then C_{SC} shall be proportional to a hyperbolic cosine (a "U"-shape function) of a linear function of an electrode surface potential (V_S):[38]

$$C_{SC} = \sqrt{\frac{4\rho\varepsilon\varepsilon_o e^2}{2kT}} \cdot \cosh\left(\frac{eV_S}{2kT}\right) \quad (1)$$

where e is the electronic charge, k is the Boltzmann's constant, T is the absolute temperature, ρ is the charge carrier density, ε is the dielectric constant of a carbon, and ε_o is the permittivity of free space.

However, for both graphite and most porous carbons (except for semiconductor single-walled carbon nanotubes, SWCNTs[39,40]), a more appropriate model might be a metal-like material with free charge carriers, but a low charge carrier density. In this case,[41]

$$C_{SC} = \sqrt{2\varepsilon\varepsilon_o} \cdot \frac{\rho(V_S)}{\sqrt{\int_0^{V_S} \rho(V)\, dV}} \quad (2)$$

where $\rho(V_s)$ is the charge carrier density, which now depends on the carbon surface potential. By applying a similar model to graphene (assuming 2D free electron gas within graphene as a model), Xia *et al.* showed that the experimentally observed "U"-shape dependence of the C_{DL} on the surface potential could be matched with such a theory quite precisely if one assumes that charge carrier density $\rho(V_s)$ in graphene has two contributions: (i) a potential-induced (induced by changes from the potential of zero charge, PZC) one and (ii) a larger one induced by defects/dopants and independent of the electrode potential.[37]

Alternative explanations have also been discussed. For example, when performing modeling on double layer formation in carbons immersed in ionic liquids, Kiyohara *et al.* and Skinner *et al.*[42] assumed that under no applied potential and even at small voltages electrolyte does not enter the small pores because the volume exclusion interactions in such pores were assumed to be so strong that they repelled ions from the pores. When increasing the applied voltage and wetting the carbon pores by electrolyte, a rapid increase in specific capacitance should thus take place, giving rise to the "U" or "dumbbell" -shape CV dependence. In other simulations, Kondrat *et al.*[25,26] assumed the opposite: complete pore filling by ionic liquid induced due to the attraction of ions to electrically conductive pores induced by the image forces. However, the authors acknowledged that both scenarios could fundamentally be plausible, depending on the energy contributions in a particular carbon/electrolyte system.

In our prior studies on the same ACF in aqueous electrolytes, we observed a near-perfect rectangular shape of the CV curves (Figure 2 of ref 30). According to our recent discussion about the pseudocapacitance detection[34] and our XPS studies (Figure 2c), we believe that these samples exhibit virtually no pseudocapacitance (which may, in principle, increase capacitance at a zero voltage, thereby flattening the CV curve). Therefore, this lack of the "U"-shape in the CVs of the ACF previously recorded in aqueous electrolytes[34] must indicate that either (i) C_{SC} is largely independent of the applied potential in aqueous electrolytes, in a direct contrast to the predictions of the eqs 1 and 2 or (ii) C_{DL} is dominated by C_e and not by C_{SC}, which is again in contradiction to most of the prior art discussions. If (i) is a correct hypothesis, then one can conclude that the potential-induced charge carrier density of ACF must remain very small within the potential range applied to electrodes so that the total number of charge carriers is mostly determined by the voltage-independent defects/dopants-induced charge carrier density. In this case a question arises: why in our organic electrolyte does the C_{SC} of the same material suddenly become voltage-dependent (see Figure 3)? Can defects/dopants-induced charge carrier density become voltage-dependent in some electrolytes? If (ii) is a correct hypothesis, then another question arises: what is the reason for the voltage dependence of C_e in our organic electrolyte? Is it possible that at least some of the smallest pores expel electrolyte (or electrolyte ions) under a zero (or small) electrode polarization, but gradually become filled with electrolyte ions upon increasing the applied voltage?

Searching for possible answers we conducted SANS studies, as described below.

SANS Analysis. Our experimental setup (Figure 4) used for *in situ* SANS analyses has been described in our prior work.[30] Briefly, ACF electrodes are placed into an optical quartz cuvette section of the hermetically sealed chamber equipped with three (3) electrical feedthroughs. Both the working and counter ACF electrodes (WE and CE) are positioned parallel to the cuvette side-to-side at a distance of $\sim$3−5 mm from each other so that the incoming neutron beam only hits the working electrode (WE), as shown in Figure 4. The diffraction patterns from the WE are then collected using a two-dimensional (2D) neutron detector, normalized to the transmission, corrected for the backgrounds (scattering from empty cell and blocked beam) and

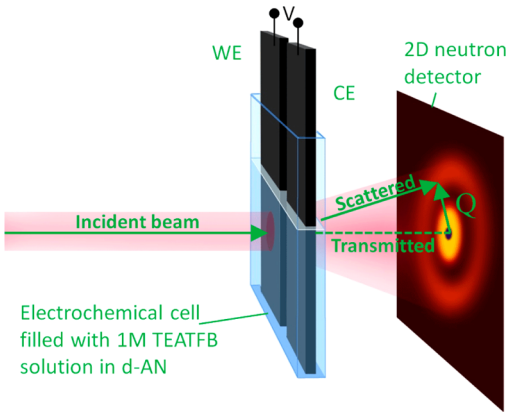

Figure 4. Schematic of the SANS measurements setup for *in situ* experimental studies of ion electrosorption phenomena in microporous carbon electrodes: the neutron beam only hits the working electrode (WE) during the collection of the scattered and transmitted neutron diffraction patterns using a 2D neutron detector. The edge of the counter electrode (CE) is located at least 5 mm away from the perimeter of the beam. The electrochemical cell is hermetically sealed (not shown for simplicity).

analyzed based on three-phase model developed and applied recently for quantifying the adsorption of supercritical fluids and gases in nanoporous materials.[43] Potentiostat controls the potential of the WE *vs* a CE or *vs* a reference electrode (RE).

Since d-AN was used in our studies, the only source of hydrogen present in the electrochemical system studied was in the $N(C_2H_5)_4^+$ cations (BF_4^- anions contain no hydrogen). The application of a positive potential results in an overall decrease in scattering intensity (black curve with black looking up triangle symbols in Figure 5a). Similarly, the application of a negative potential results in an overall increase in scattering intensity (blue curve with blue looking down triangle symbols in Figure 5a). Such trends could be expected since the H-containing TEATFB cations must be electrosorbed into the pores under application of a negative potential, and expelled (replaced) with the non-hydrogen containing anions and solvent molecules at a positive potential. In addition, due to approximately 20% of the BF_4^- anions containing neutron-absorbing B10, the neutron scattering intensity is attenuated with the higher presence of BF_4^- anions in the pores. This will strengthen the overall trends observed by ~32% according to our calculations conducted considering the number of H and B atoms in each ion and the values for the neutron scattering and attenuation cross sections, respectively. The application of a positive potential fills the pores with higher concentrations of BF_4^- anions, resulting in a further overall decrease in scattering intensity. The application of a negative potential reduces the concentration of BF_4^- anions in the pores, resulting in an overall further increase in scattering intensity. The observations of the shifts in scattering intensity with the applied voltages validate our methodology and

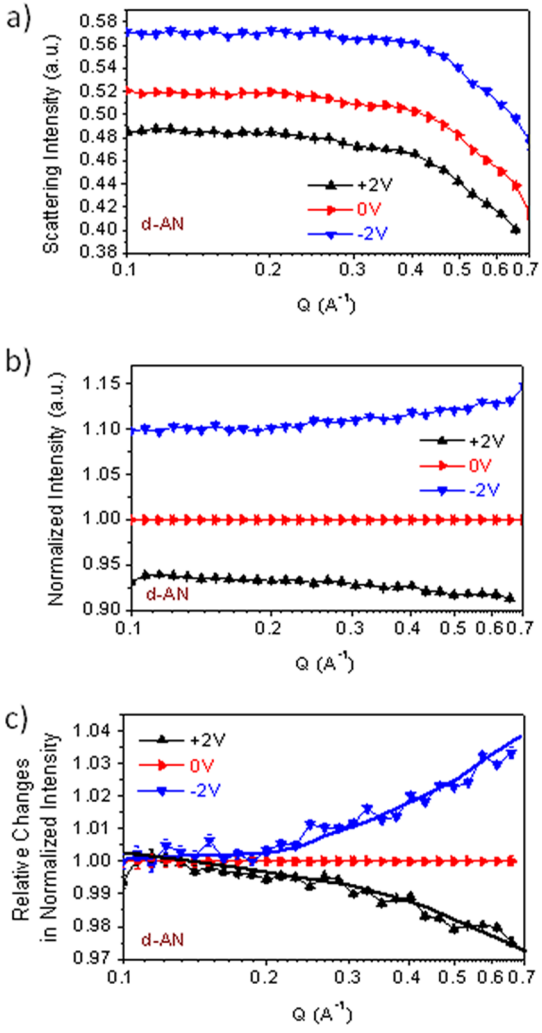

Figure 5. *In situ* neutron scattering experiments on ACF electrodes immersed into 1 M TEATFB/d-AN electrolyte under an application of a potential between the WE and CE: (a) SANS patterns, (b) SANS profiles normalized by the 0 V one, (c) relative changes in the intensity of the normalized SANS profiles.

corroborate trends we observed in our previous studies with aqueous solutions.[30]

To gain insights into the adsorption of ions within the pores of different sizes, we normalized the SANS intensities to a zero voltage SANS profile (Figure 5b). Under the application of −2 V, the scattering intensity increases by ~10%, which could be approximated as the H enrichment of 7.5% within the relatively large pores. Under the application of +2 V, the scattering intensity decreases by ~7%, which manifests the H depletion of 5%. A slightly larger increase in the scattering intensity under a negative potential than the corresponding decrease under a positive potential could be related to slightly higher initial concentration of BF_4^- anions in carbon pores. The smallest pores ($Q > 0.2$ Å^{-1}) of ACF exhibit even higher ion adsorption capacity, as manifested by higher scattering intensities for these pores, indicative of higher H concentration

and lower B10 concentration at negative potentials, and lower scattering intensities for these pores, indicative of lower H concentration and higher B10 concentration at positive potentials. Figure 5c, where relative changes in the normalized scattering intensities are shown for both the negative and positive potentials applied to the ACF WE, shows the effect of pore size on ion electroadsorption even more clearly. The statistical uncertainties of the reported results (error bars indicated) are smaller than the trends observed. Such finding indeed supports many previously reported results that indicated the possible enhancement of organic electrolyte ion adsorption in the small subnanometer pores of many porous carbon materials.[5,6]

These results are also in line with our previous SANS studies of ion adsorption in H_2SO_4 solutions in H_2O, where electrolyte was found to completely wet the carbon surface, including the smallest pores.[30] However, as previously discussed, we observed greatly diminished proton adsorption in such pores if the electrolyte solvent did not wet them, as in the case of a D_2O-based electrolyte.[30] Therefore, we were highly interested to identify if d-AN would penetrate into the smallest pores.

To answer this important question, we conducted SANS measurements on dry ACF and on ACF infiltrated with d-AN. By deconvoluting the total scattering patterns into the scattering from the fiber outer surfaces, scattering from pores and incoherent background we could identify the degree of pore filling over a broad pore size range.[30] If d-AN completely and uniformly wetted all the pores, we would see a parallel vertical downshift of the ACF scattering curve at all *Q*-values with some normalization factor (due to smaller contrast between carbon and deuterated solvents than between carbon and air). But in contrast to our expectation, we observed that the saturation of ACF with d-AN leads to a *Q*-dependent decrease in the scattering intensity (Figure 6), indicating that a significant portion of the smallest pores ($Q > 0.2$ Å^{-1}) is not completely filled with d-AN and thus exhibits a stronger scattering intensity. Since the molecular radius of the d-AN molecule is ~2.1 Å,[44,45] it is not expected that the size of the d-AN molecule will limit access to the smallest pores (~0.5 nm in size). Thus, this incomplete wetting likely originates from the high carbon/d-AN interfacial energy, which may prevent the electrolyte access to the smallest pores.

To independently confirm the lack of complete wetting of ACF, we have conducted d-AN solvent infiltration/displacement experiments, where we measured the mass (and thus volume) of d-AN displaced by ACF. Assuming the "true density" of carbon in ACF to be in the range of 2−2.2 g/cm^3, we estimate that at least 0.05−0.1 cm^3/g of ACF pore volume remains solvent-free. From the observations of both (i) ion enrichment in the smallest ($Q > 0.2$ Å^{-1}) pores under applied potential (Figure 5c) and (ii) the absence of electrolyte in such pores under no potential (Figure 6), we conclude that the application of potential to ACF electrodes induces electrowetting of d-AN-based electrolyte. Furthermore, such a conclusion may additionally explain the "butterfly wing" shape of the CV curve because higher surface area becomes accessible for ion storage at higher voltages (Figure 3). Since the smallest electrolyte-free pores (Figure 6) are expected to exhibit the highest area-normalized capacitance,[16] electrowetting such pores may, in principle, account for the ~30% observed increase in capacitance at 2 V (Figure 3). Therefore, our results may challenge the universality of a commonly accepted model of a carbon space charge dependence on the applied voltage, initially proposed to explain the CV shape.

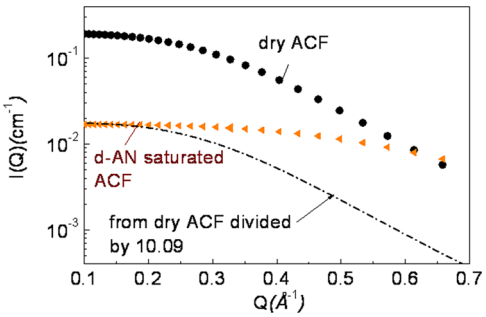

Figure 6. Neutron scattering experiments on dry ACF electrodes as well as on ACF immersed into d-AN: neutron scattering from micropores in the studied samples. The dash line represents scattering from dry ACF normalized by 0.0991 to a maximum intensity of the neutron scattering curves of ACF immersed into d-AN.

Several factors may explain significantly stronger electrowetting of d-AN-based electrolytes compared with previously reported D_2O-based electrolytes.[30] First, one should expect that a higher interfacial energy between a polar D_2O and a hydrophobic carbon surface (compared to that between a less polar d-AN and carbon) should create a stronger energy barrier to overcome during electrowetting. Second, we observe that increase in capacitance at higher voltages becomes more pronounced at above 0.5−0.6 V (Figure 3) when we apply larger potential (up to 2 V in case of d-AN-based electrolyte *vs* 0.6 V in case of D_2O-based electrolyte). This higher potential provides stronger driving force for filling electrolyte-depleted regions within carbon nanopores.

CONCLUSIONS

Potential-dependent electroadsorption of $N(C_2H_5)_4^+$ cations and BF_4^- anions in acetonitrile solution by binder-free microporous activated carbon fabric electrodes was studied by a combination of electrochemical measurements and *in situ* SANS technique using a custom-built hermetic apparatus. TEM and Raman spectroscopy measurements confirmed highly disordered microstructure of the studied material, while XPS showed

minimal content of functional groups present on the carbon surface. Nitrogen sorption measurements showed pores within 0.4−2.2 nm, similar to that of activated carbons used in commercial devices. Cyclic voltammetry measurements showed a "butterfly wing" shape of the CV curves, which is often observed in high surface area carbon materials and commonly explained by the gradual increase in a carbon space charge at higher applied voltages. We have demonstrated for the first time the unique ability of SANS to monitor organic electrolyte ion adsorption in carbon pores as a function of the applied potential and pore size. Furthermore, our *in situ* SANS measurements revealed that ion adsorption is strongly enhanced in the smallest subnanometer pores, in spite of their incomplete wetting by the electrolyte solvent. Therefore, an alternative explanation to the characteristic shape of the CV was proposed: electrowetting of the smallest pores at increasing device potentials. The methodology outlined in this paper can be used to investigate and compare ion adsorption in various other organic electrolytes and porous carbons with different microstructure, shape and size of the pores and surface chemistry for gaining better fundamental understanding of ion sorption phenomena for energy storage and other applications.

METHODS

Commercially available ACF (ACC-507-20) were purchased from Kynol and used to analyze electrosorption of ions in organic electrolytes. For electrochemical testing, the activated carbon fabric of ~300 μm in average thickness was cut into strips of approximately 1 cm in width. Four strips were used for WE and CE in *in situ* experiments. These tests were performed in a symmetric two-electrode configuration using hermetically sealed beaker-type cells (Figure 1) assembled in a He-filled glovebox. For *ex situ* electrochemical experiments, the electrodes and separator (Whatman grade GF/B glass microfiber filter) were dried under vacuum at 110 °C for 24 h and assembled in CR2016 coin cells in an Ar-filled glovebox. For the *ex situ* experiments, we performed tests to measure response of the WE individually while ensuring a minimal cross-contamination of organic solvents. Throughout the course of these experiments, one electrolyte was investigated: 1 M tetraethyl ammonium tetrafluoroborate (TEATFB, Sigma Aldrich) which was diluted to 1 M concentration in deuterated acetonitrile (99.96%, Cambridge Isotope Laboratories).

Electrochemical characterization of ACF was performed using cyclic voltammetry (CV). Cyclic voltammetry was performed using a Gamry Potentiostat with the potential being swept from 0.0 to 2.0 V at scan rates of 1−1000 mV·s^{-1}. The integrated-average gravimetric capacitance of each electrode was calculated from the CV data (in symmetric, two-electrode configuration) according to

$$C_{\text{electrode}} = 2C_{\text{cell}} = \left(\frac{2}{(\mathrm{d}U/\mathrm{d}t)\cdot m}\right)\cdot\left\{\int_{0\,\mathrm{V}}^{2.0\,\mathrm{V}} I(U)\,\mathrm{d}U - \int_{2.0\,\mathrm{V}}^{0\,\mathrm{V}} I(U)\,\mathrm{d}U\right\}\cdot\frac{1}{2}\cdot\frac{1}{2V} \quad (3)$$

where dU/dt is the scan rate, m is the mass of each electrode in a symmetric cell, and $I(U)$ is the total current. The capacitance of each electrode was calculated from the CV data according to

$$C_{\text{electrode}} = \left(\frac{I(U)}{(\mathrm{d}V/\mathrm{d}t)\cdot m}\right) \quad (4)$$

where dV/dt is the instantaneous scan rate at the WE measured with the respect to the CE, m is the mass of each electrode, and $I(U)$ is the total current.

Scanning electron microscopy (SEM) measurements were performed using a LEO 1550 microscope (Carl Zeiss, Germany).

XPS was performed on a Kratos Axis Ultra with an Al kα X-ray source. An Ar filled sample transport chamber was used to prevent air exposure between drying and analysis. The sample was dried at 150 °C overnight, and loaded into the transport chamber in an Ar filled glovebox. The elliptical analysis spot size was ~300 × 700 μm. The detector pass energy was set to 80 eV for the survey spectrum and 20 eV for the high resolution spectrum, with a step size of 0.1 eV.

TEM experiments were performed on a High-Resolution Transmission Electron Microscope (FEI Tecnai F30, accelerating voltage of 300 kV).

SANS experiments were conducted at ORNL General Purpose SANS instrument with a neutron wavelength of λ = 4.75 Å and a wavelength spread, $\Delta\lambda/\lambda$ of 0.13. Two sample-to-detector distances, 10 and 0.3 m, were used to cover a Q range between Q_{min} of 0.008 Å^{-1}, and Q_{max} of 0.9 Å^{-1}, where $Q = 4\pi\sin(\theta)/\lambda$ is the scattering vector and 2θ is the scattering angle. The sample-to-detector distance was chosen to cover a broad range of scattering vectors Q up to 0.9 Å^{-1}. Average acquisition time for each scattering curve was approximately 60 min. Scattering patterns were corrected for instrumental background, the transmission and detector efficiency. The raw 2D data were azimuthally averaged to produce the 1D profile, $I(Q)$ *versus* Q. The data were placed on an absolute scale (cm^{-1}) using precalibrated standards. The measurements were conducted at room temperature. SANS patterns were recorded from dry ACF electrodes, ACF infiltrated with d-AN and with 1 M TEATFB/d-AN electrolyte at different applied voltages to monitor the changes in the distribution of hydrogen ion concentrations as a function of pore size. For the solvent-wetting measurement, the ACF sample was immersed in the solvent for 24 h before the measurement. ACF samples were sealed in the quartz sample holders with internal thickness 2 mm. The following equation was used for the deconvolution of the scattering intensity patterns into three terms:

$$I(Q) = \frac{A}{Q^n} + \frac{C}{1+(|Q-Q_0|\xi)^m} + B \quad (5)$$

where the first term describes the scattering from the fiber surface (A is a constant and n is the fractal dimension), the second term describes the scattering from meso- and micropores (C is a constant, Q_0 is the position of the maximum, which is related to the characteristic spacing ξ between pores, and m is the Lorentzian exponent) and the constant B represents the incoherent background.

The normalized SANS intensities were obtained by dividing the scattering intensities measured at a certain potential ($I(Q,V)$ by the scattering intensities measured at zero potential $I(Q,V = 0)$ as

$$I_{\text{normalized}}(Q,V) = I(Q,V)/I(Q,V=0) \quad (6)$$

The relative changes in the normalized intensity as a function of scattering vector were obtained by subtracting the normalized scattering intensity measured at Q = 0.4 Å from the normalized intensity:

$$\Delta I_{\text{normalized}}(Q,V) = I(Q,V)/I(Q,V=0) - I_{\text{normalized}}(0.4\ \text{Å}^{-1},V) \quad (7)$$

This procedure was selected to show Q-domain (Q > 0.4 Å^{-1}) corresponding to subnanometer pores in which the variation of the normalized intensity is most pronounced.

The statistical uncertainty of normalized intensity was calculated as follows:

$$\frac{\delta I_{\text{normalized}}(Q,V)}{I_{\text{normalized}}(Q,V)} = \sqrt{\left(\frac{\delta I(Q,V)}{I(Q,V)}\right)^2 + \left(\frac{\delta I(Q,V=0)}{I(Q,V=0)}\right)^2} \quad (8)$$

where $\delta I(Q,V)$ is the measured uncertainty.

Conflict of Interest: The authors declare no competing financial interest.

Acknowledgment. This research was supported by the Army Research Office (ARO grant W911NF-12-1-0259). The research at ORNL's High Flux Isotope Reactor was sponsored by the Laboratory Directed Research and Development Program and the Scientific User Facilities Division, Office of Basic Energy Sciences, U.S. Department of Energy. The TEM work presented here was performed on equipment supported by funding from NSF DMR 0922776.

REFERENCES AND NOTES

1. Gu, W.; Yushin, G. Review of Nanostructured Carbon Materials for Electrochemical Capacitor Applications. *Wiley Interdiscip. Rev.: Energy Environ.* **2013**, 10.1002/wene.102.
2. Miller, J. R.; Simon, P. Materials Science—Electrochemical Capacitors for Energy Management. *Science* **2008**, *321*, 651–652.
3. Wei, L.; Yushin, G. Nanostructured Activated Carbons from Natural Precursors for Electrical Double Layer Capacitors. *Nano Energy* **2012**, *1*, 552–565.
4. Salitra, G.; Soffer, A.; Eliad, L.; Cohen, Y.; Aurbach, D. Carbon Electrodes for Double-Layer Capacitors. I. Relations between Ion and Pore Dimensions. *J. Electrochem. Soc.* **2000**, *147*, 2486–2493.
5. Chmiola, J.; Yushin, G.; Gogotsi, Y.; Portet, C.; Simon, P.; Taberna, P. L. Anomalous Increase in Carbon Capacitance at Pore Sizes Less Than 1 Nanometer. *Science* **2006**, *313*, 1760–1763.
6. Raymundo-Pinero, E.; Kierzek, K.; Machnikowski, J.; Beguin, F. Relationship between the Nanoporous Texture of Activated Carbons and their Capacitance Properties in Different Electrolytes. *Carbon* **2006**, *44*, 2498–2507.
7. Portet, C.; Yushin, G.; Gogotsi, Y. Electrochemical Performance of Carbon Onions, Nanodiamonds, Carbon Black and Multiwalled Nanotubes in Electrical Double Layer Capacitors. *Carbon* **2007**, *45*, 2511–2518.
8. Gu, W. T.; Peters, N.; Yushin, G. Functionalized Carbon Onions, Detonation Nanodiamond and Mesoporous Carbon as Cathodes in Li-Ion Electrochemical Energy Storage Devices. *Carbon* **2013**, *53*, 292–301.
9. Rose, M.; Korenblit, Y.; Kockrick, E.; Borchardt, L.; Oschatz, M.; Kaskel, S.; Yushin, G. Hierarchical Micro- and Mesoporous Carbide-Derived Carbon as High Performance Electrode Material in Supercapacitors. *Small* **2011**, 1108–1117.
10. Stoeckli, F.; Centeno, T. A. Pore Size Distribution and Capacitance in Microporous Carbons. *Phys. Chem. Chem. Phys.* **2012**, *14*, 11589–11591.
11. Centeno, T. A.; Stoeckli, F. The Volumetric Capacitance of Microporous Carbons in Organic Electrolyte. *Electrochem. Commun.* **2012**, *16*, 34–36.
12. Lee, S. I.; Saito, K.; Kanehashi, K.; Hatakeyama, M.; Mitani, S.; Yoon, S. H.; Korai, Y.; Mochida, I. B-11 NMR Study of the BF4- Anion in Activated Carbons at Various Stages of Charge of EDLCs in Organic Electrolyte. *Carbon* **2006**, *44*, 2578–2586.
13. Wang, H.; Koster, T. K. J.; Trease, N. M.; Segalini, J.; Taberna, P. L.; Simon, P.; Gogotsi, Y.; Grey, C. P. Real-Time NMR Studies of Electrochemical Double-Layer Capacitors. *J. Am. Chem. Soc.* **2011**, *133*, 19270–19273.
14. Borchardt, L.; Oschatz, M.; Paasch, S.; Kaskel, S.; Brunner, E. Interaction of Electrolyte Molecules with Carbon Materials of Well-Defined Porosity: Characterization by Solid-State NMR Spectroscopy. *Phys. Chem. Chem. Phys.* **2013**, *15*, 15177–15184.
15. Deschamps, M.; Gilbert, E.; Azais, P.; Raymundo-Pinero, E.; Ammar, M. R.; Simon, P.; Massiot, D.; Beguin, F. Exploring Electrolyte Organization in Supercapacitor Electrodes with Solid-State NMR. *Nat. Mater.* **2013**, *12*, 351–358.
16. Huang, J. S.; Sumpter, B. G.; Meunier, V. Theoretical Model for Nanoporous Carbon Supercapacitors. *Angew. Chem., Int. Ed.* **2008**, *47*, 520–524.
17. Huang, J. S.; Sumpter, B. G.; Meunier, V. A Universal Model for Nanoporous Carbon Supercapacitors Applicable to Diverse Pore Regimes, Carbon Materials, and Electrolytes. *Chem.—Eur. J.* **2008**, *14*, 6614–6626.
18. Feng, G.; Qiao, R.; Huang, J. S.; Sumpter, B. G.; Meunier, V. Ion Distribution in Electrified Micropores and Its Role in the Anomalous Enhancement of Capacitance. *ACS Nano* **2010**, *4*, 2382–2390.
19. Vatamanu, J.; Borodin, O.; Smith, G. D. Molecular Dynamics Simulations of Atomically Flat and Nanoporous Electrodes with a Molten Salt Electrolyte. *Phys. Chem. Chem. Phys.* **2010**, *12*, 170–182.
20. Jiang, D. E.; Jin, Z. H.; Wu, J. Z. Oscillation of Capacitance inside Nanopores. *Nano Lett.* **2011**, *11*, 5373–5377.
21. Yang, L.; Fishbine, B. H.; Migliori, A.; Pratt, L. R. Molecular Simulation of Electric Double-Layer Capacitors Based on Carbon Nanotube Forests. *J. Am. Chem. Soc.* **2009**, *131*, 12373–12376.
22. Merlet, C.; Rotenberg, B.; Madden, P. A.; Taberna, P. L.; Simon, P.; Gogotsi, Y.; Salanne, M. On the Molecular Origin of Supercapacitance in Nanoporous Carbon Electrodes. *Nat. Mater.* **2012**, *11*, 306–310.
23. Xing, L. D.; Vatamanu, J.; Borodin, O.; Bedrov, D. On the Atomistic Nature of Capacitance Enhancement Generated by Ionic Liquid Electrolyte Confined in Subnanometer Pores. *J. Phys. Chem. Lett.* **2013**, *4*, 132–140.
24. Fedorov, M. V.; Georgi, N.; Kornyshev, A. A. Double Layer in Ionic Liquids: The Nature of the Camel Shape of Capacitance. *Electrochem. Commun.* **2010**, *12*, 296–299.
25. Kondrat, S.; Georgi, N.; Fedorov, M. V.; Kornyshev, A. A. A Superionic State in Nano-Porous Double-Layer Capacitors: Insights from Monte Carlo Simulations. *Phys. Chem. Chem. Phys.* **2011**, *13*, 11359–11366.
26. Kondrat, S.; Kornyshev, A. Superionic State in Double-Layer Capacitors with Nanoporous Electrodes. *J. Phys.: Condens. Matter* **2011**, 23.
27. Arulepp, A.; Permann, L.; Leis, J.; Perkson, A.; Rumma, K.; Janes, A.; Lust, E. Influence of the Solvent Properties on the Characteristics of a Double Layer Capacitor. *J. Power Sources* **2004**, *133*, 320–328.
28. Tamai, H.; Kunihiro, M.; Morita, M.; Yasuda, H. Mesoporous Activated Carbon as Electrode for Electric Double Layer Capacitor. *J. Mater. Sci.* **2005**, *40*, 3703–3707.
29. Kotz, R.; Hahn, M.; Gallay, R. Temperature Behavior and Impedance Fundamentals of Supercapacitors. *J. Power Sources* **2006**, *154*, 550–555.
30. Boukhalfa, S.; He, L.; Melnichenko, Y. B.; Yushin, G. Small Angle Neutron Scattering for the *in Situ* Probing of Ion Adsorption Inside Micropores. *Angew. Chem., Int. Ed.* **2013**, *52*, 4618–4622.
31. Wei, L.; Nitta, N.; Yushin, G. Lithographically Patterned Thin Activated Carbon Films as a New Technology Platform for On-Chip Devices. *ACS Nano* **2013**, *7*, 6498–6506.
32. Wei, L.; Sevilla, M.; Fuertes, A. B.; Mokaya, R.; Yushin, G. Polypyrrole-Derived Activated Carbons for High-Performance Electrical Double-Layer Capacitors with Ionic Liquid Electrolyte. *Adv. Funct. Mater.* **2012**, *22*, 827–834.
33. Wei, L.; Sevilla, M.; Fuertesc, A. B.; Mokaya, R.; Yushin, G. Hydrothermal Carbonisation of Abundant Renewable Natural Organic Chemicals for High-Performance Supercapacitor Electrodes. *Adv. Energy Mater.* **2011**, *1*, 356–361.
34. Gu, W. T.; Sevilla, M.; Magasinski, A.; Fuertes, A. B.; Yushin, G. Sulfur-Containing Activated Carbons with Greatly Reduced Content of Bottle Neck Pores for Double-Layer Capacitors: A Case Study for Pseudocapacitance Detection. *Energy Environ. Sci.* **2013**, *6*, 2465–2476.
35. Hahn, M.; Baertschi, M.; Barbieri, O.; Sauter, J. C.; Kotz, R.; Gallay, R. Interfacial Capacitance and Electronic Conductance of Activated Carbon Double-Layer Electrodes. *Electrochem. Solid-State Lett.* **2004**, *7*, A33–A36.

36. Gerischer, H.; McIntyre, R.; Scherson, D.; Storck, W. Density of the Electronic States of Graphite—Derivation from Differential Capacitance Measurements. *J. Phys. Chem.* **1987**, *91*, 1930–1935.
37. Xia, J. L.; Chen, F.; Li, J. H.; Tao, N. J. Measurement of the Quantum Capacitance of Graphene. *Nat. Nanotechnol.* **2009**, *4*, 505–509.
38. Randin, J. P.; Yeager, E. Differential Capacitance Study on Basal Plane of Stress-Annealed Pyrolytic-Graphite. *J. Electroanal. Chem.* **1972**, *36*, 257–276.
39. Yamada, Y.; Kimizuka, O.; Tanaike, O.; Machida, K.; Suematsu, S.; Tamamitsu, K.; Saeki, S.; Yamada, Y.; Hatori, H. Capacitor Properties and Pore Structure of Single- and Double-Walled Carbon Nanotubes. *Electrochem. Solid-State Lett.* **2009**, *12*, K14–K16.
40. Yamada, Y.; Tanaka, T.; Machida, K.; Suematsu, S.; Tamamitsu, K.; Kataura, H.; Hatori, H. Electrochemical Behavior of Metallic and Semiconducting Single-Wall Carbon Nanotubes for Electric Double-Layer Capacitor. *Carbon* **2012**, *50*, 1422–1424.
41. Gerischer, H. An Interpretation of the Double-Layer Capacity of Graphite-Electrodes in Relation to the Density of States at the Fermi Level. *J. Phys. Chem.* **1985**, *89*, 4249–4251.
42. Skinner, B.; Chen, T.; Loth, M. S.; Shklovskii, B. I. Theory of Volumetric Capacitance of an Electric Double-Layer Supercapacitor. *Phys. Rev. E* **2011**, *83*, 056102.
43. Melnichenko, Y. B.; Mayama, H.; Cheng, G.; Blach, T. Monitoring Phase Behavior of Sub- and Supercritical CO_2 Confined in Porous Fractal Silica with 85% Porosity. *Langmuir* **2009**, *26*, 6374–6379.
44. Boes, E. S.; Livotto, P. R.; Stassen, H. Solvation of Monovalent Anions in Acetonitrile and N,N-Dimethylformamide: Parameterization of the IEF-PCM Model. *Chem. Phys.* **2006**, *331*, 142–158.
45. Roy, S.; Komath, S.; Bagchi, B. Molecular Theory of Ultrafast Solvation in Liquid Acetonitrile. *J. Chem. Phys.* **1993**, *99*, 3139–3142.